Hindawi
International Journal of Aerospace Engineering
Volume 2021, Article ID 8843453, 16 pages
https://doi.org/10.1155/2021/8843453

Research Article

A Computational Design Analysis of UAV's Rotor Blade in Low-Temperature Conditions for the Defence Applications

Sreenadh Chevula,[1] **Sankeerth Chillamcharal**,[2] **and Satya Prasad Maddula**[1]

[1]*Department of Aerospace Engineering, GITAM (Deemed to be University), Rudraram Mandal, Sangareddy, District, Patancheru, Hyderabad, Telangana 502329, India*
[2]*Collins Aerospace, Embassy Tech Village Road 2B, Tower 3 4th Floor, Building No. 797, Devarabisanahalli, Bellandur, Bengaluru, Karnataka 560103, India*

Correspondence should be addressed to Sreenadh Chevula; schevula@gitam.edu

Received 16 September 2020; Revised 6 November 2020; Accepted 23 November 2020; Published 6 January 2021

Academic Editor: Jacopo Serafini

This paper discusses about the critical situations faced by the Defence operations with drones in the area of Siachen Glacier in the Himalayas. The reasons for the structural failures in drone's rotor blades and the low-performance efficiency of the drones at low-temperature conditions are highlighted. A possible solution to the above-mentioned problems has been addressed by introducing a new boundary design in the rotor blades and composite materials. The results which are shown in this paper are obtained by the computational analysis facility located at the Department of Aerospace Engineering, School of Technology, GITAM (Deemed to be University), Hyderabad. By mimicking the Siachen Glacier atmosphere conditions, the proposed rotor blade design has been analysed in CFD.

1. Introduction

Unmanned air vehicles (UAV) and drones play a major role in various Defence operations, namely in remote sensing, surveillance, and data collection in the critical areas. In such operations, the lifetime of the drones plays a major role. It is a fact that various parameters of the drone's operational conditions show huge influence on the performance and structural integrity of the drones. In terms of structural components, the main component of the drones and most of the UAV are rotor blades, and in the design of these blades, the condition of the operational temperature is one of the major parameter. As a study of temperature influence and to overcome the structural failures in the rotor blades, in this paper, the case study of Siachen Glacier is under the India Army control [1], located at 35.421226° N, 77.109540° E. The glacier is nothing but moving location of densely formed ice which has been classified by their thermal characteristics, morphology, and behaviour [2]. The selected location map of the Siachen Glacier can be found in Figure 1 [3].

The temperature conditions (see Figure 2) [4, 5] for the proposed work in this paper have been identified from the Siachen Glacier with latitude 35,500000 | 35, 30.000000 N | N35 30 00; longitude 77.000000 | 77 0.000000E | E0 77 00 00; and field elevation 22,000 ft/6706 m MSL. In the selected area, the winter snow fall will approximately 35 ft from the surface and the temperature can drop up to -50°C (-58°F).

Considering the applications of UAV and drones in glacier conditions, world widely, many studies had been conducted, such as analysing the snow depth [6–9]. A low-cost UAV has been used to test the SFM performance in topographic and lighting conditions of different types of snows which has been discussed in Cimoli et al. [6]. A comparison of photogrammetric maps collected by the UAV has been performed by Avanzi et al. [10]. A flow velocity over glacier land has been conducted by Jones C et al. [11]. Another studies relevant to identifying and analysing changes of surface features such as ice cliffs have been conducted by Steiner, J.F. et. al., Buri, P et al., and Brun, et al. [12–14],

Figure 1: Map location of Siachen Glacier [3].

Figure 2: Location of Siachen Glacier [4, 5].

Beyond various studies conducted by worldwide researchers in terms of durability and structural integrity of the UAV's and drones in glacier conditions, this paper focuses on the computational design analysis of rotor blades (further mentioned as propellers in this paper). An existing propeller blade design (Design-1) and proposed new designs (Design-2) and (Design-3) are created in Catia V5 (geometry information can be found in the following sections), and computational analysis and results are obtained by using ANSYS 16.0. A comparison between the results obtained from the computational analysis of Design-1 (existing rotor blade model), Design-2, and Design-3 (Proposed model) is shown in "Obtained Results." Finally, conclusions has been plotted in "Conclusion."

2. Designing the Solution

Several methods are used to calculate the performance parameters of a propeller, namely, momentum theories [15], blade element theories [16], hybrid blade element momentum theories [17, 18], and lifting line theories [19]. Without computational analysis, using some specified mathematical models will give the values of few propeller performance parameters. But in terms of high accuracy and optimization of the procedures, some new methods have been introduced which can be obtained only by using computational analysis. It is a well-known fact that a propeller acts like a rotating wing, and its cross-section is an airfoil. In terms of optimizing, a propeller performance optimizes the airfoil shapes used along the blade span, and an optimization of an airfoil shape can be challenging, if the shape is described using individual points. A common approach to describing the number of parameters used to describe an airfoil is to parameterize the shape. A study can be found with respective to the common approach can be found in Kulfan et al. [20]. This approach has been adopted in this paper and aimed at studying the propeller optimization with a coupled electric motor, and also, a hybrid blade element momentum theory has been proposed to estimate the propeller performance analysis.

The lifting surface on a propeller is called a blade, and a propeller can have any number of blades. Most propellers have two to four blades. Any given point along a blade the cross-section has all the same characteristics as an airfoil such as leading and trailing edges, mean camber line, chord line, and thickness, where the blades connect is called the hub which is directly attached either to an engine or to a transmission. The root is the area between the hub and the blade, and the tip is end of the blade opposite the hub, as shown in Figure 3 [21, 22] and Figure 4 [21, 22]. The propeller performance parameters, namely, the *blade angle*, β, is the "resultant angle between the free stream and rotational velocity components," the *effective pitch*, p_e, is "the distance a propeller advances in one rotation," the *geometric pitch*, g_e, is "the theoretical distance an element of a propeller blade would travel in one rotation"(g_e is not constant along the length of blade), and *the advance ratio*, J, is "the ratio between the distance the propeller moves forward through one rotation and the blade diameter."

$$J = \frac{V}{nD}, \tag{1}$$

where n is in rotations per second, V is the velocity, and D is the diameter of the blade); the *aspect ratio* (AR) is the tip radius divided by the maximum blade width. A spinner is a conical or parabolic shaped fairing that is mounted over the canter of the centre of the propeller where it is connected to the hub, the *thrust or driving face* is the blade face is the lower surface of the propeller airfoil, and the *blade back* is the upper surface of the propeller. Most of the parameters can be visually found in Figure 5.

Based on the operational areas of the drones or UAV, propellers are classified in four ways, namely, tractor, pusher propellers (based on thrust production), and fixed and variable pitched propellers (based on the pitch geometry). A variable pitch propeller's blades can be adjusted either on the ground or during fight to allow the propeller to operate at maximum performance throughout its operation range.

As mentioned above, to obtain the propeller performance parameters values with more accuracy, several computational

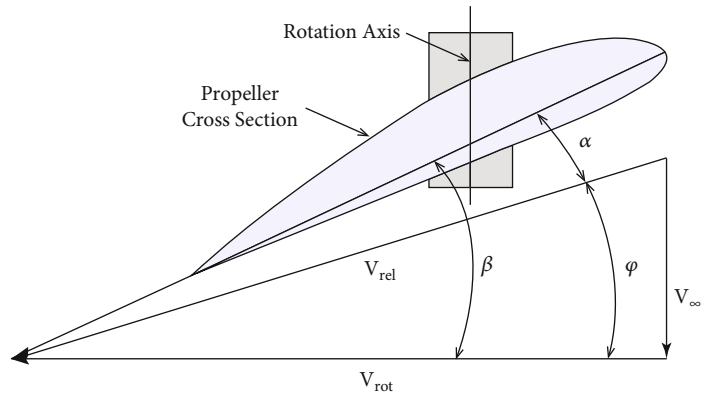

Figure 3: Cross-section of the blade with velocity diagram [21, 22].

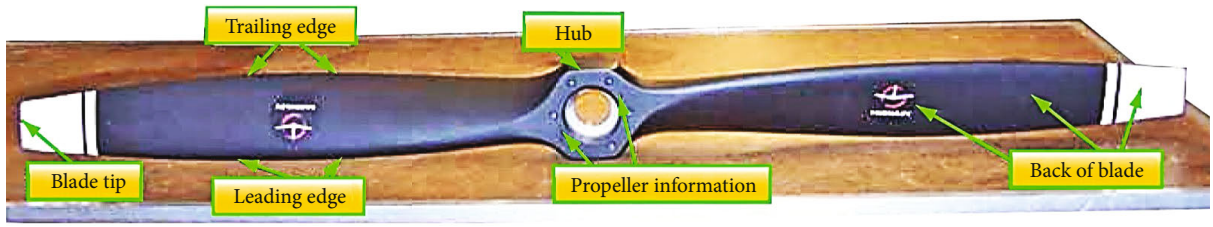

Figure 4: Basic nomenclature of propellers [24].

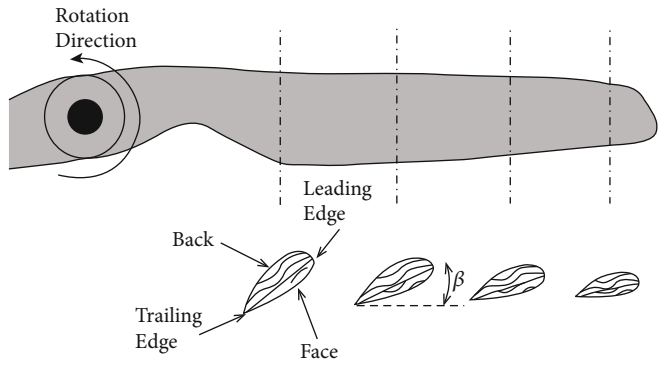

Figure 5: Cross-sections of the propeller blade [21, 22].

methods are used in the design of propellers, which will utilizes some nondimensional numbers, namely, the thrust coefficient C_t, power coefficient, C_q, and the efficiency η.

$$C_t = \frac{F_t}{\rho n^2 D^4}, \tag{2}$$

$$C_q = \frac{Q}{\rho n^3 D^5}, \tag{3}$$

$$\eta = \frac{C_t J}{C_P}, \tag{4}$$

where n is the rotation speed, D is the diameter of the propeller, ρ is the density of air, and J is the advance ratio.

3. Blade Element Rotor Theory

In the propeller performance parameters analysis, the blade element theory is one of the simplest method. A relatively simple method of predicting the more detailed performance of a helicopter rotor using blade element theory can be found in ref [23]. From Figures 6 and 7, the difference in angle between thrust and lift directions is defined as

$$\varphi = \theta - \alpha, \tag{5}$$

where θ is the geometric pitch angle, α is the angle of attack with respective to the flow, and φ is the difference between the angles.

V_0 is the axial flow at propeller disk, V_1 is the section local flow velocity vector, summation of vectors V_0 and V_2, and V_2 is the angular flow velocity vector.

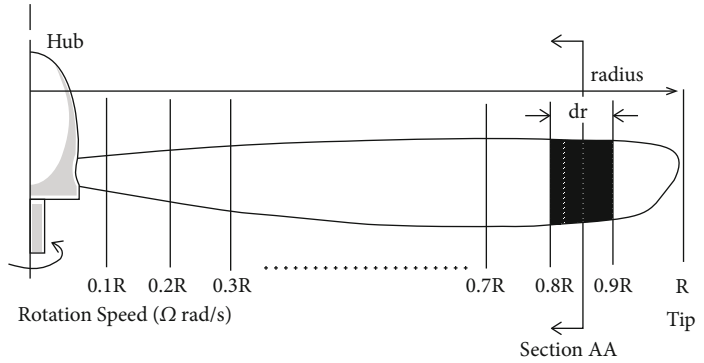

Figure 6: Blade element subdivision [23].

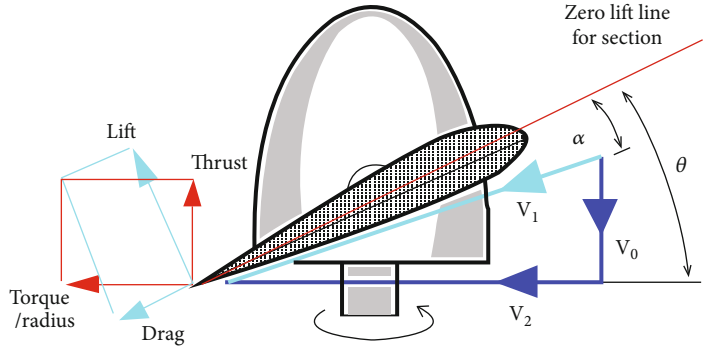

Figure 7: Resultant of force vectors and flow vectors [23].

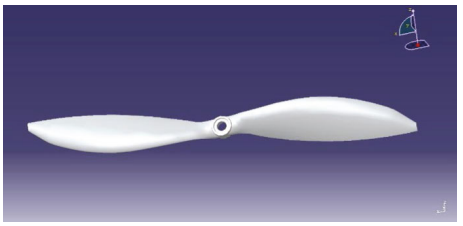

Figure 8: Design-1.

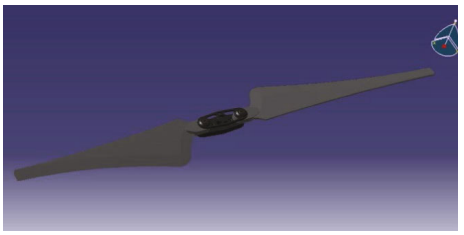

Figure 9: Design-2.

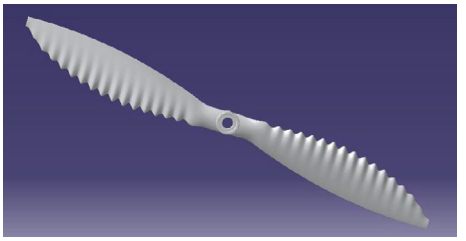

Figure 10: Design-3.

Table 1: The geometry design of propellers.

Name	Diameter in m	Pitch	Amplitude	Frequency
Design-1	0.254	0.1778	N/A	N/A
Design-2	0.254	0.1778	N/A	N/A
Design-3	0.254	0.1778	1c	20w

The elemental thrust and torque of this blade element can thus be written as

$$\Delta T = \Delta L \cos(\varphi) - \Delta D \sin(\varphi),$$
$$\frac{\Delta Q}{r} = \Delta D \cos(\varphi) + \Delta L \sin(\varphi). \quad (6)$$

Case 1. For a single blade.

Substituting section data (C_L and C_D for the given α) then

$$\Delta L = C_L \frac{1}{2} \rho V_I^2 c.dr,$$
$$\Delta D = C_D \frac{1}{2} \rho V_I^2 c.dr, \quad (7)$$

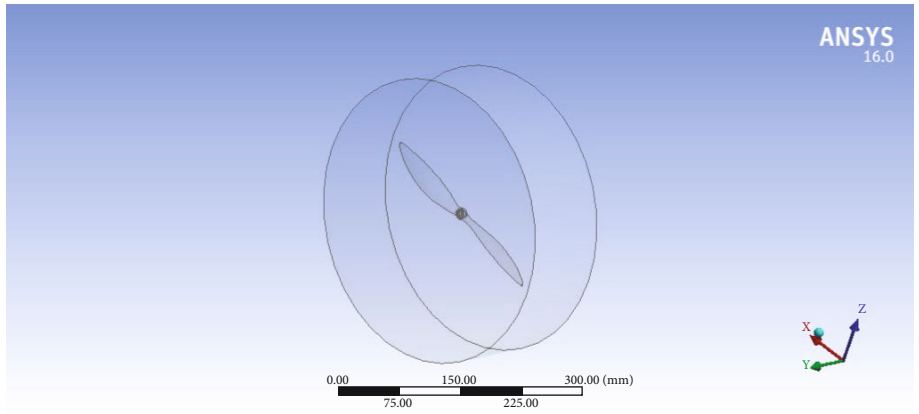

Figure 11: Rotation domain of Design-1.

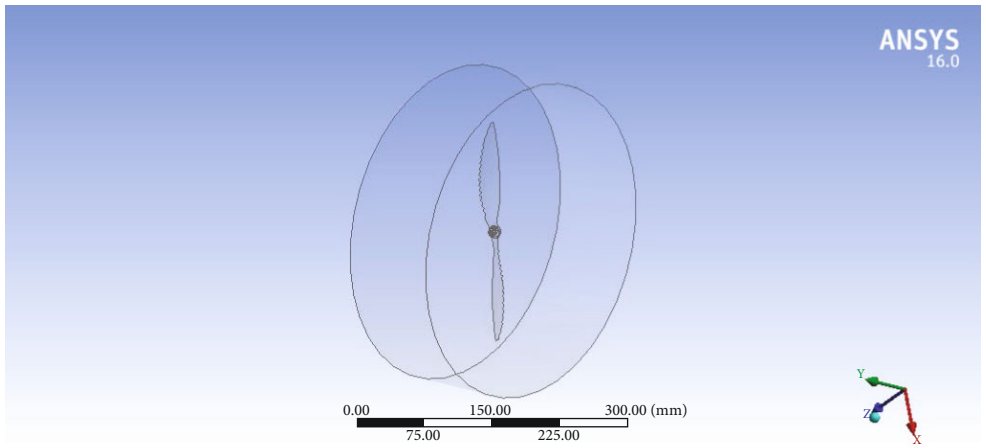

Figure 12: Rotation domain of Design-2.

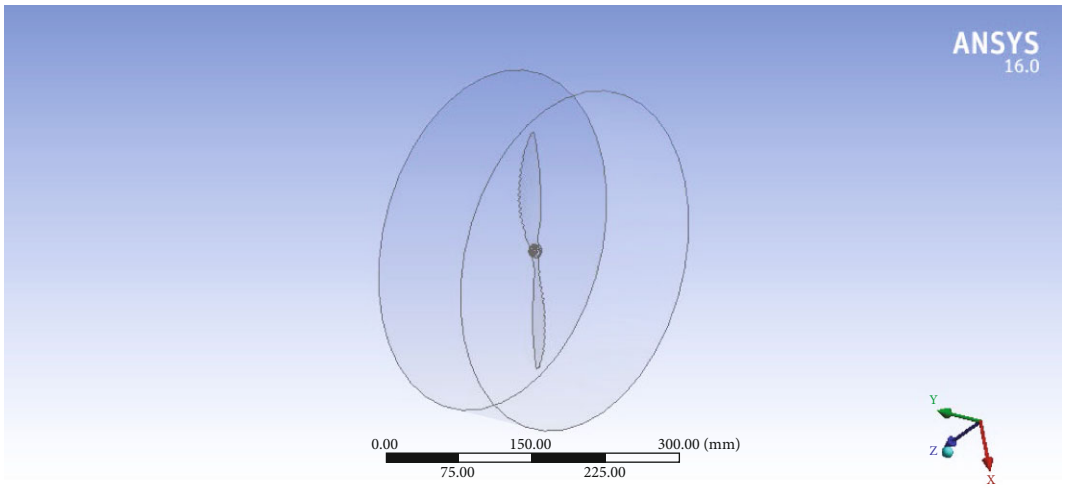

Figure 13: Rotation domain of Design-3.

where ρ is the air density, and c is the blade chord so that the lift producing area of the blade element is $c.dr$.

Case 2. If the number of propeller blades is B then the area generating the lift will be the element area multiplied by the number of blades B covering the circuit, and the lift coefficient can be assumed to be linear.

$$\Delta T = \frac{1}{2}\rho V_I^2 c(C_L \cos(\varphi) - C_D \sin(\varphi))B.dr \quad , \qquad (8)$$

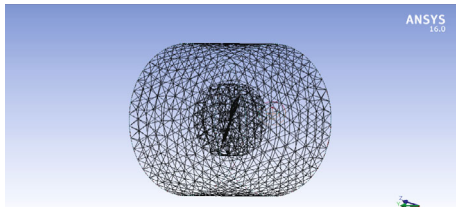

Figure 14: Design-1 (generated mesh). Mesh type: unstructured tetrahedral mesh. Nodes: 120561. Elements: 81184.

$$\Delta T = \frac{1}{2}\rho V_I^2 c(C_D \cos(\varphi) - C_L \sin(\varphi))B.dr \quad . \tag{9}$$

The overall propeller thrust and torque can be found by the summation of the radial blade element values, i.e.,

$$T = \Sigma\Delta T \text{ (for all elements) and } Q = \Sigma\Delta Q \text{ (for all elements)}. \tag{10}$$

The relation between nondimensional thrust (C_p) and torque coefficients (C_t) and the efficiency of the propeller (η) and advance ratio J can be found in Equations (1), (2), (3), and (4). The blade element theory is an iterative solution procedure and starts with an initial guess of induced flow component V_I. With the guess of V_I, the flow angle on the blade will be estimated, and based on the use of blade section properties, the element thrust and torque will be estimated. The approximated values obtained from the guessed values and the force balance can be used to give improved estimates of the induced velocity V_I. Until the value of V_I got converged to within a specified tolerance, the iteration process will be continued. (It should also be noted that convergence for a nonlinear system of equations is not guaranteed.) In this paper, linear airfoil section properties have been used to design propellers. So to obtain required results, a convergence enhancing technique (Crank-Nicholson underrelaxation) has been proposed to use.

4. Computational Analysis of the Propellers

Various experimental and computational analysis are available to obtain the results of the propeller analysis. Firstly, in an experimental method, the propeller blades will be tested in both static and advancing flow conditions in a wind tunnel setup. Secondly, in a computational analysis adopts three-dimensional computational fluid dynamics (CFD) simulation, utilizing the Reynolds-average Navier–Stokes (RANS) equation. CFD tools are the useful tools for propeller design and analysis. In this paper, a flow simulation (under low-temperature conditions) on propeller blades is proposed to conduct by using ANSYS 16.0. The geometry conditions of propellers Design-1 (Figure 8), Design-2 (Figure 9), and Design-3 (Figure 10) can be found in Table 1. In general, the standard geometry of the propellers has a 0.254 m diameter. So in this paper, for computational design, approximate values of 0.254 m in diameter propellers have been designed in Catia V5.

In the above given three designs, the pitch of 0.1778 m provides a pitch-to-diameter ratio of 0.7, which is common for an off-shelf propeller type. The value of the Reynolds number for the testing flow condition is proposed to set for 50804 which can be obtained by a rotational speed of the propeller 3008 RPM and 75% of blade station from the chord.

5. Computational Setup

The computational predictions have been obtained from the ANSYS 16.0 CFD solver. The approach of the multiple reference frame model (MRF) has been incorporated to obtain the predicted flow around the propellers which can be shown in the following figures (see Figures 11–13). The computational domain has been split into a global, rotating region, and local domains. The rotational domain can be found where the propeller blade and hub enclosed without openings (see Figures 11–13).

Considering the full development (without any unexpected interruptions) of the upstream and downstream flow simulations and results around the propellers, a good configuration of the flow domain plays a major role in the computational setup. In this line, for the proposed computational setup of this paper, the stationary regions inlet and outlet boundaries are located at 4D from the origin of the propellers, and the enclosure of the rotating domain is set to be 1.1D and 0.4D.

Grid generation is another important factor to obtain good and accurate results in computational analysis. The rate of convergence, computational time, and performance depends on the quality of the computational grid generation. In this paper, the mesh grid has been generated using Ansys FLUENT 16.0 (see Figures 14–17). The cell size of the mesh kept smaller size or range around the propeller blade in rotational domain. From the rotational domain, a gradual increment in cell size towards the stationary region has been implemented in the grid generation with enough grid refinements across the interface.

In the computational analysis, especially in the grid generation, most of the researchers will select the unstructured tetrahedral grids because of its compatibility to solve complex geometries by discretizing. This paper also selected unstructured tetrahedral grids in the grid generation. Table 2 shows the details of the grid generation of this work.

6. Obtained Results

Defence operational conditions for UAV such as operational altitude, geographical areas, and mission operational profiles can be found in Figure 18.

Operational Area Siachen Glacier is known as the world's highest battlefield, and soldiers have been deployed at an elevation of up to 6000 m (19685 feet) from sea level. In this paper, based on the operational temperature with respective change in the altitudes (with gradual increment of 250) (see Figure 18), the vertical drone operational area has been divided in to five zones. Complete information about the five zones, temperature, and required RPM of the Drone propellers can be found in Table 3.

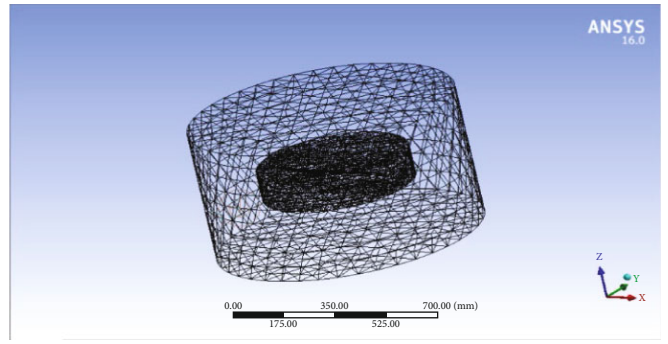

Figure 15: Design-2 (generated mesh). Mesh type: unstructured tetrahedral mesh. Nodes: 759610. Elements: 482119.

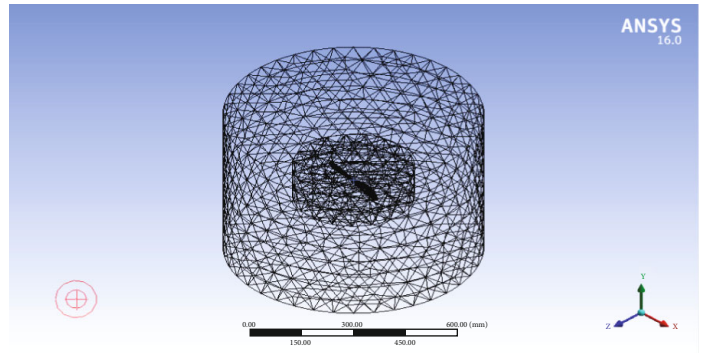

Figure 16: Design-3 (generated mesh). Mesh type: unstructured tetrahedral mesh. Nodes: 120561. Elements: 81184.

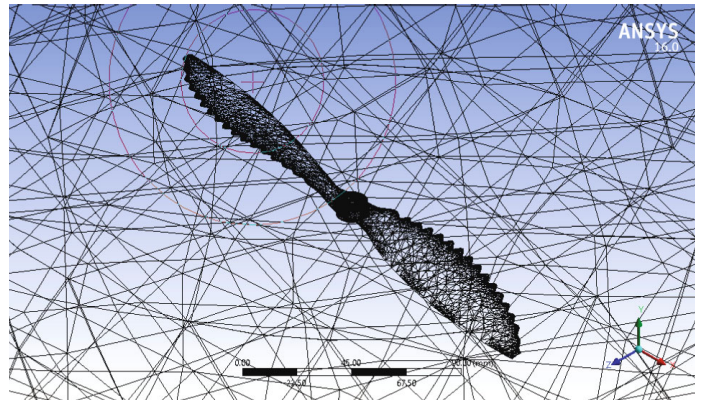

Figure 17: Design-3 (internal view of mesh). Mesh type: unstructured tetrahedral mesh. Nodes: 120561. Elements: 81184.

Table 2: The parameters of the grid generation.

Use advance size function	Curvature
Relevance centre	Coarse
Curvature normal angle	70.9
Min size	0.589180
Max face size	50.9180
Max size	117.840
Growth rate	1.850
Minimum edge length	$1.507e-002$

6.1. Pressure Contour for Propeller Design-1 (Zone-1 to Zone-5), Respectively. For the mimicking condition of Zone-1 with 0°C and velocity of 8 m/s obtained by 5000 RPM, the results of the pressure contour influence vary from the hub to the tailing edge of the rotor ($-3.651e+003$ to $8.385e+002$ Pa).

For the mimicking condition of Zone-2 with -25°C and velocity of 8 m/s obtained by5500 RPM, the results of the pressure contour influence vary from the hub to the tailing edge of the rotor ($-3.48e+003$ to $9.796e0+002$ Pa).

For the mimicking condition of Zone-3 with -50°C and velocity of 8 m/s obtained by6000 RPM, the results of the pressure contour influence vary from the hub to the tailing edge of the rotor ($-4.34e+003$ to $8.796e0+002$ Pa).

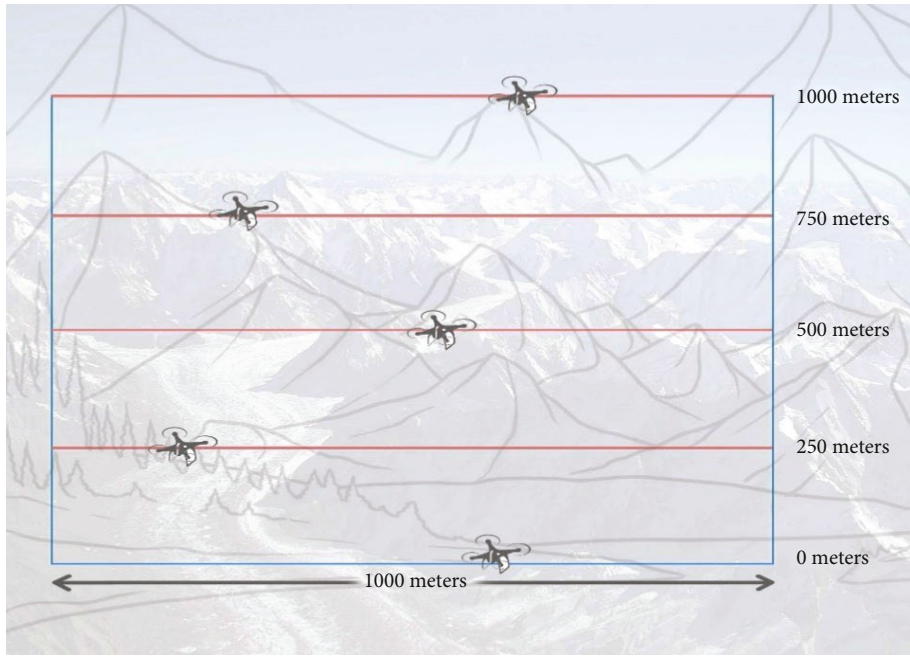

Figure 18: Operational mission profile.

Table 3: Operational mission profile.

	∗Altitudes (m)	∗ Temperature	RPM drone	Velocity (m/s)
Zone-1	0	0	5000	8
Zone-2	250	-25°C	5500	8
Zone-3	500	-50°C	6000	8
Zone-4	750	-75°C	6500	8
Zone-5	1000	-100°C	7000	8

∗The altitude and temperatures are taken from above 6000 m from the sea level.

For the mimicking condition of Zone-4 with -75°C and velocity of 8 m/s obtained by6500 RPM, the results of the pressure contour influence vary from the hub to the tailing edge of the rotor ($-4.17e + 003$ to $1.129e0 + 002$ Pa).

For the mimicking condition of Zone-5 with -100°C and velocity of 8 m/s obtained by7000 RPM, the results of the pressure contour influence vary from the hub to the tailing edge of the rotor ($-5.33e + 003$ to $1.30e0 + 003$ Pa).

Note: the obtained pressure contour for the propeller Design-2 (Zone-1 to Zone-5) is almost similar to Design-1. So those results are not shown in this paper.

6.2. Pressure Contour for Propeller Design-3 (Zone-1 to Zone-5), Respectively. For the mimicking condition of Zone-1 with -0°C and velocity of 8 m/s obtained by5000 RPM, the results of the pressure contour influence vary from the hub to the tailing edge of the rotor ($-2.42e + 003$ to $1.434e0 + 003$ Pa).

For the mimicking condition of Zone-2 with -25°C and velocity of 8 m/s obtained by5500 RPM, the results of the pressure contour influence vary from the hub to the tailing edge of the rotor ($-2.74e + 003$ to $1.722 + 003$ Pa).

For the mimicking condition of Zone-3 with -50°C and velocity of 8 m/s obtained by6000 RPM, the results of the pressure contour influence vary from the hub to the tailing edge of the rotor ($-3.09e + 003$ to $2.03e0 + 003$ Pa).

For the mimicking condition of Zone-4 with -75°C and velocity of 8 m/s obtained by6500 RPM, the results of the pressure contour influence vary from the hub to the tailing edge of the rotor ($-3.65e + 003$ to $2.39e0 + 003$ Pa).

For the mimicking condition of Zone-5 with -100°C and velocity of 8 m/s obtained by7000 RPM, the results of the pressure contour influence vary from the hub to the tailing edge of the rotor ($-4.24e + 003$ to $2.78e0 + 003$ Pa).

With the gradual increment in the RPM obtained the required velocity of 8 m/s with respect to the increments in the zone's altitude (Zone-1 to Zone-5). The influence of the pressure distribution from the leading edge to the tailing edge in Design-1 and Design-3 has a drastic change, and finally, the proposed Design-3 performed smooth pressure distribution profiles (Figures 19–22) in all operational conditions which are simulated for Siachen Glacier geographical location.

6.3. Results with Respect to the Influencing Parameters. The obtained results with respect to the drone's performance influencing the parameters of Design-1, Design-2, and Design-3 are summarized (see Equations (1)–(4) and Equation (9)) in the tables and the graphical representation.

From Figure 23, we can find that Design-3 and Design-2 have a similar performance at temperature -25°C. But in

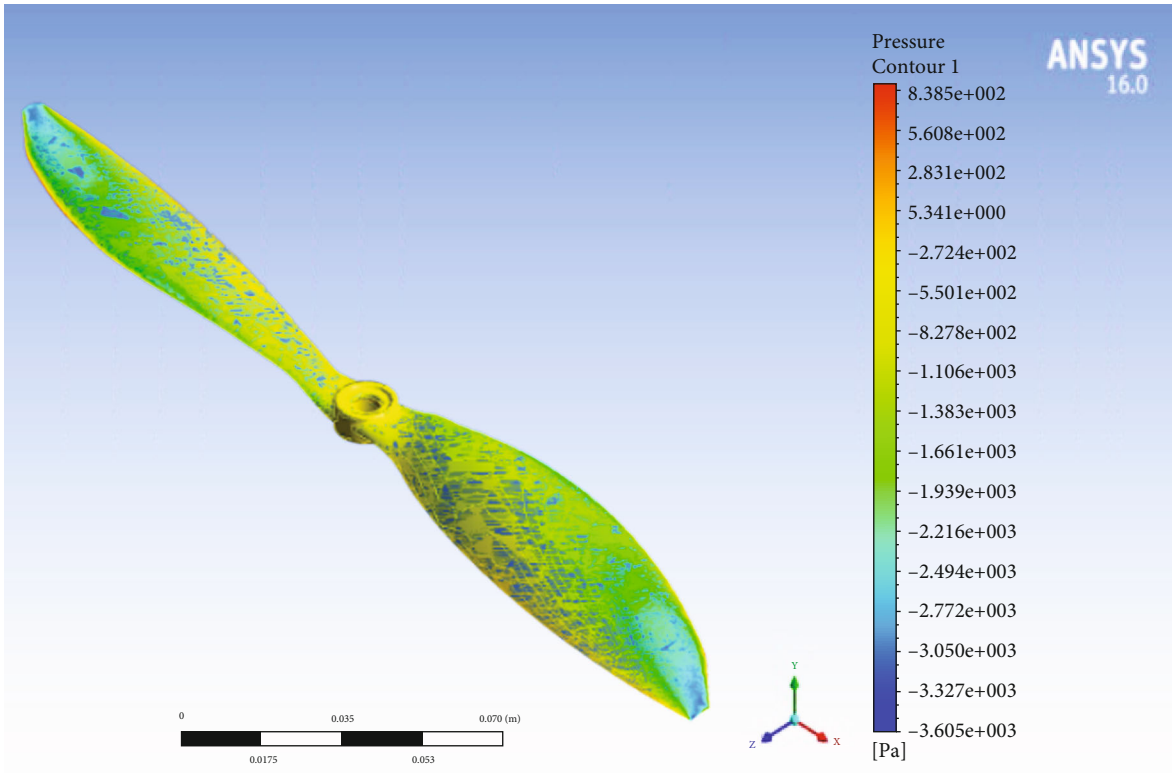

Figure 19: Pressure contour at 0°C temperature.

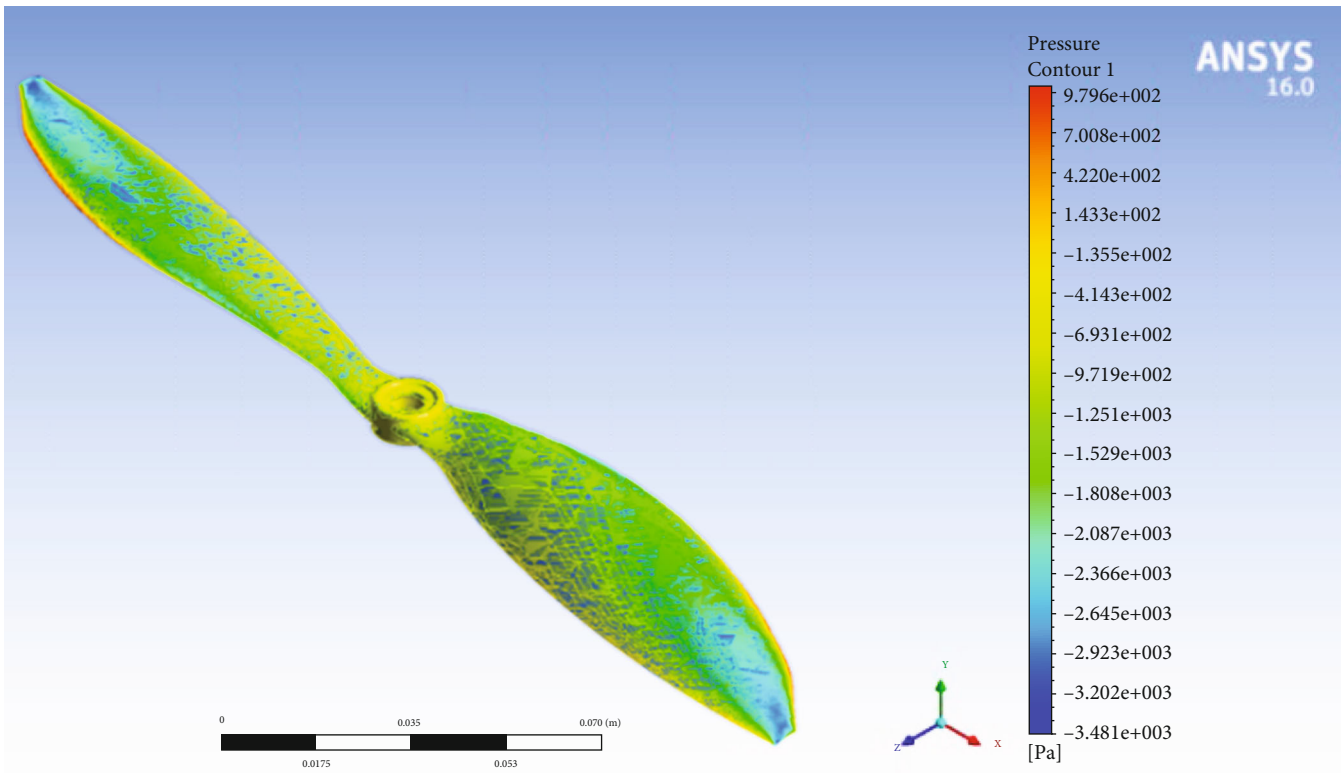

Figure 20: Pressure contour at -25°C temperature.

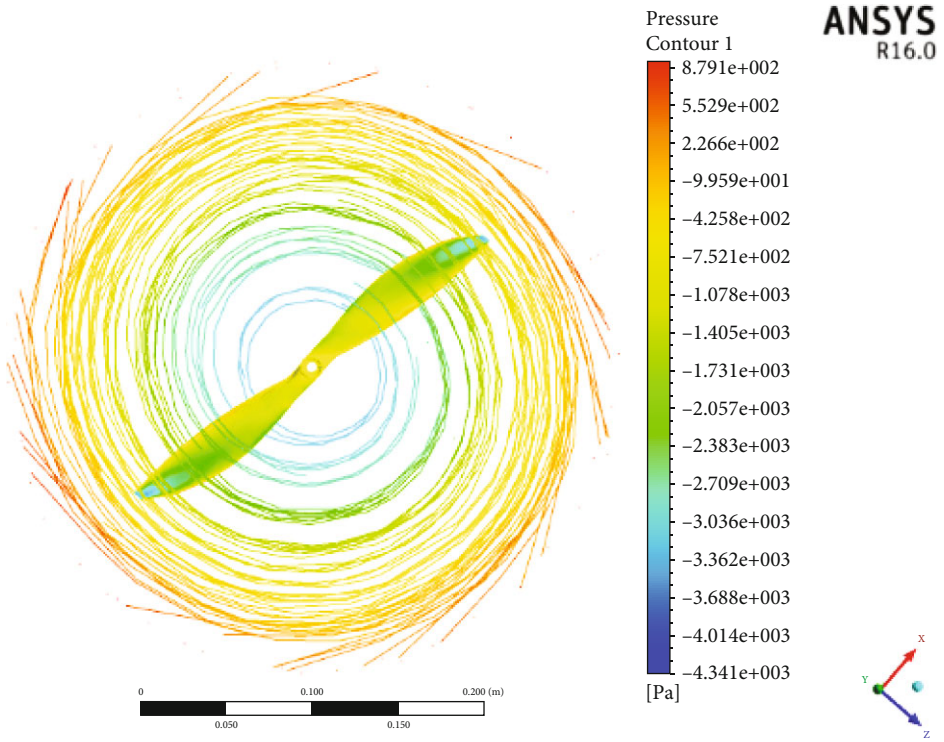

Figure 21: Pressure contour at -50°C temperature.

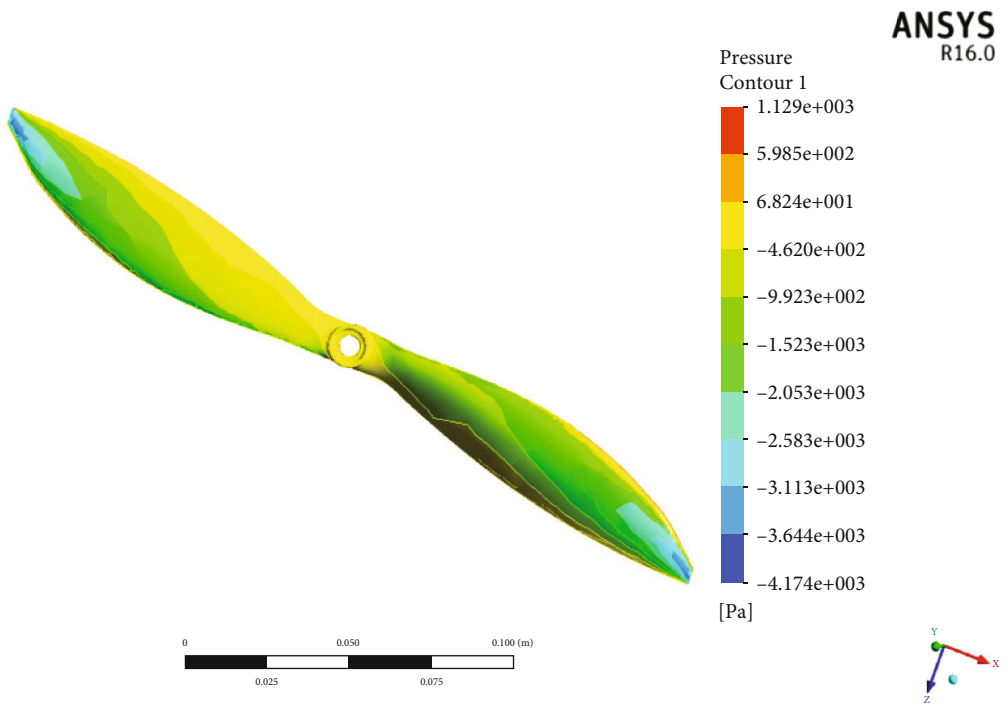

Figure 22: Pressure contour at -75°C temperature.

other temperature conditions, low performance has been identified due to its geometrical design conditions. Finally, the proposed Design-3 results the better performance in the comparison of existing Design-1 and Design-2 with respect to the all operational conditions which are simulated for Siachen Glacier geographical location.

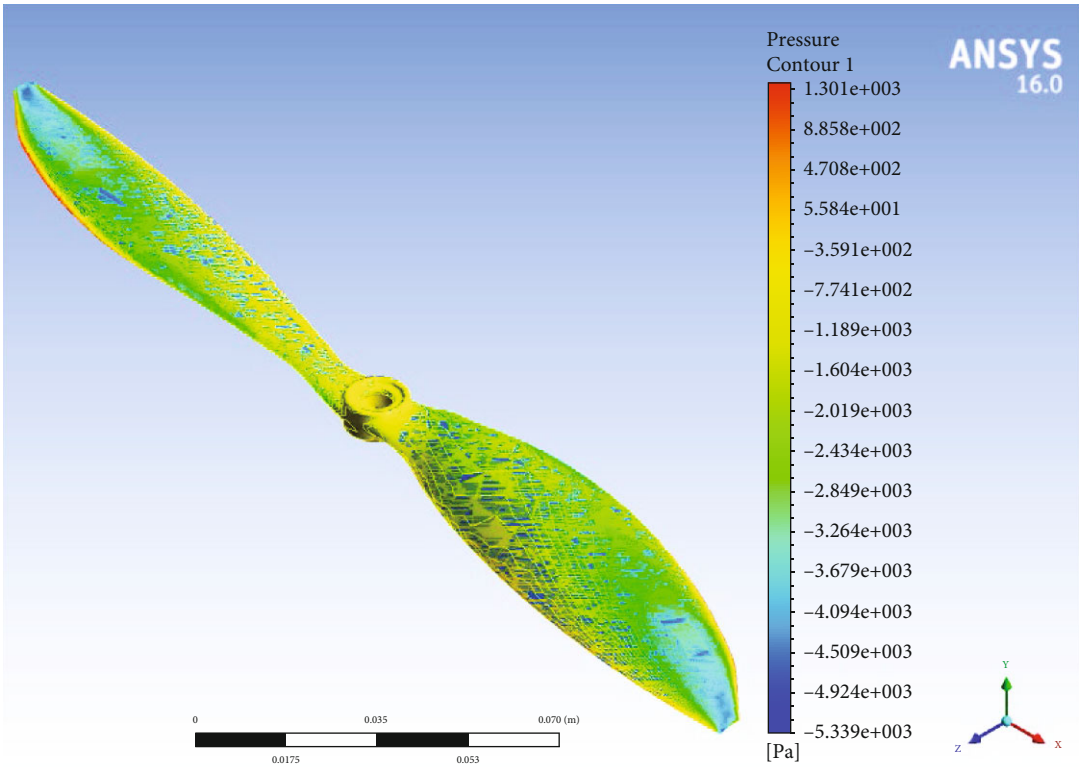

Figure 23: Pressure contour at -100°C temperature.

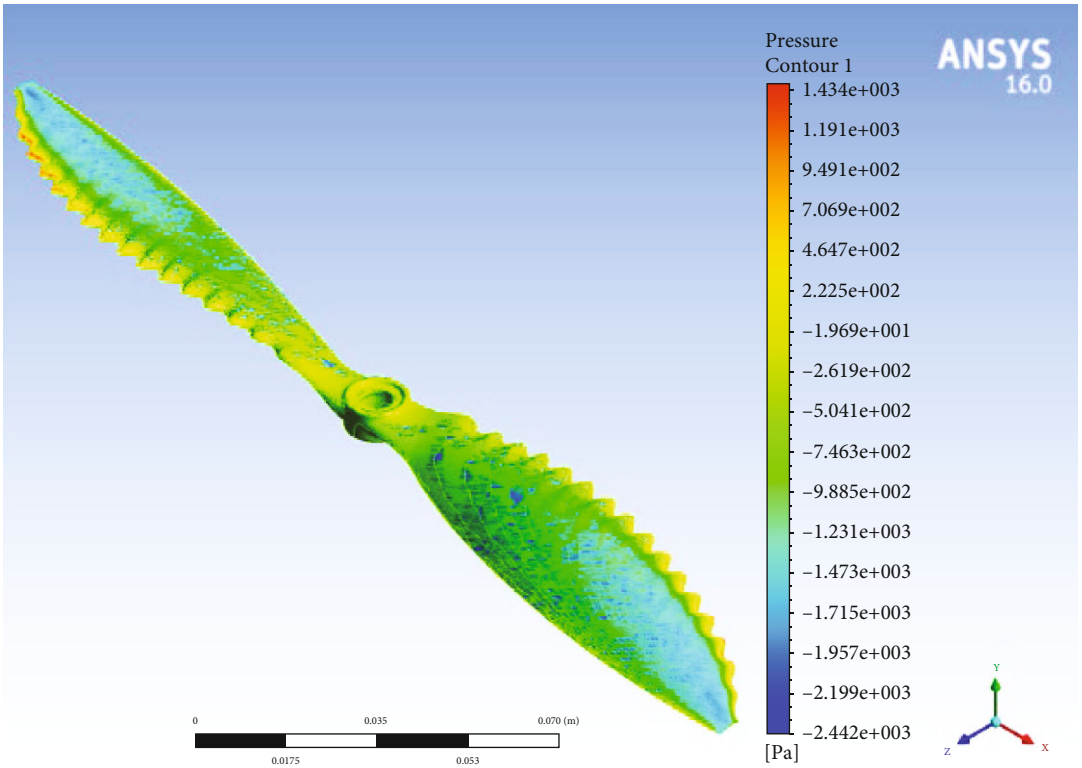

Figure 24: Pressure contour at 0°C temperature.

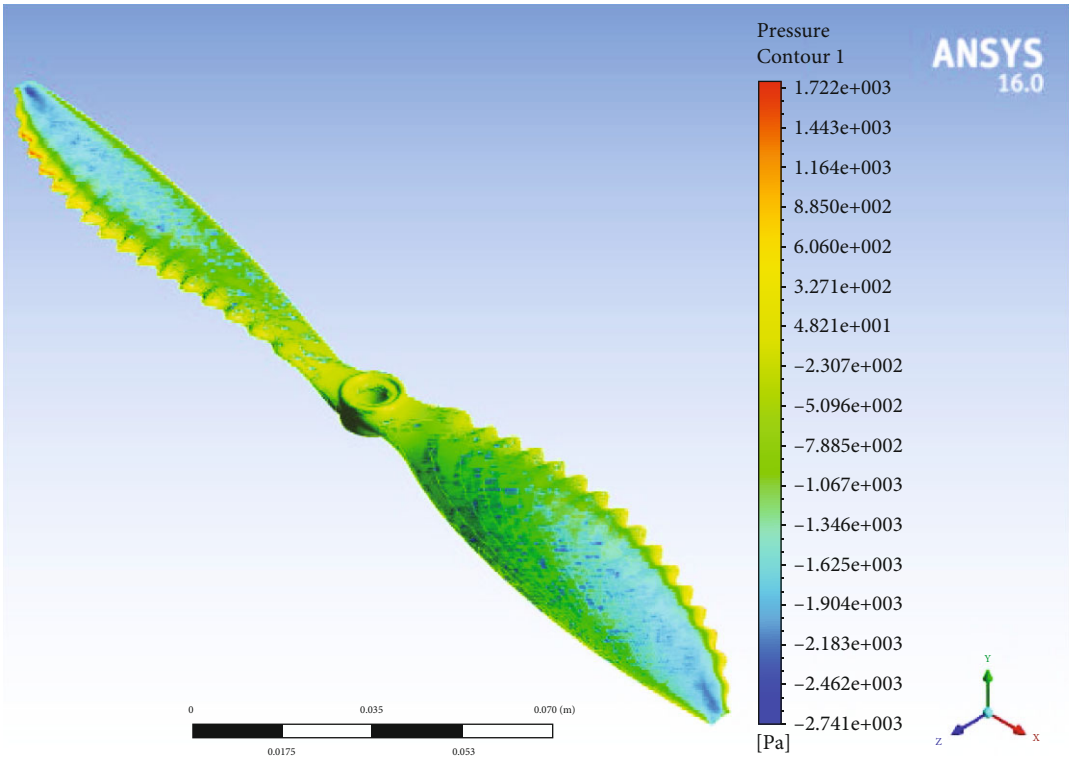

Figure 25: Pressure contour at -25°C temperature.

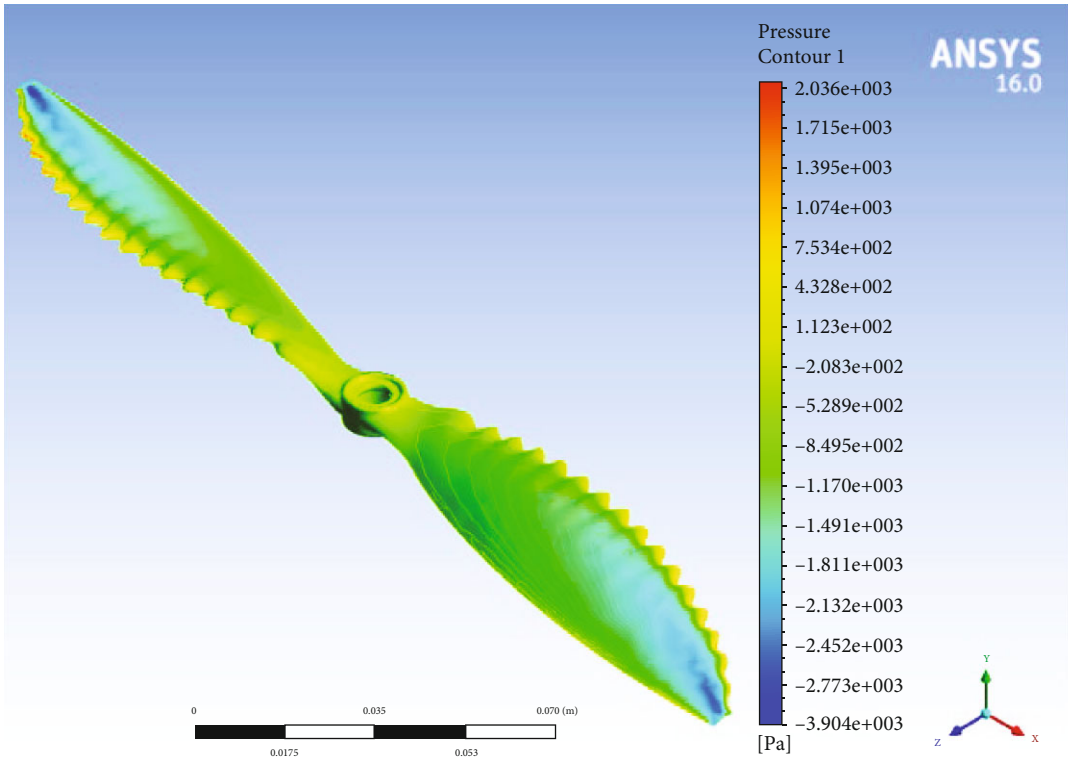

Figure 26: Pressure contour at -50°C temperature.

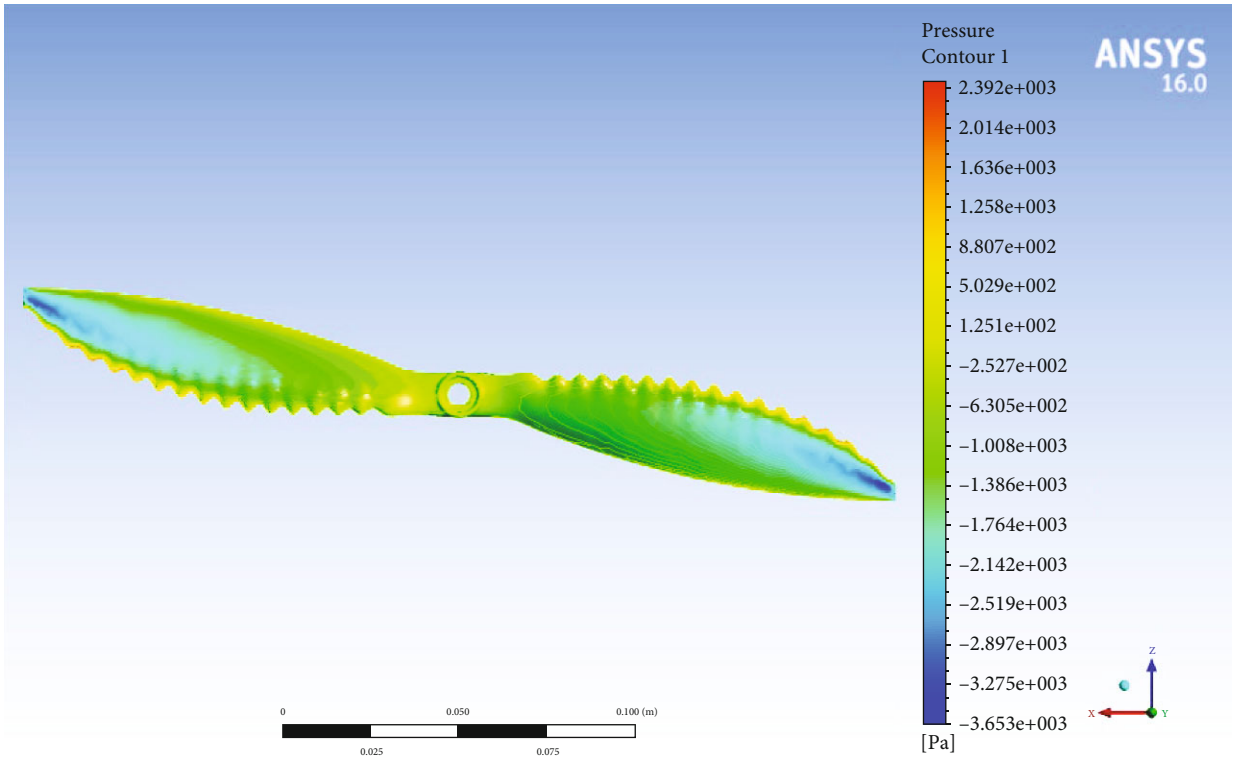

Figure 27: Pressure contour at -75°C temperature.

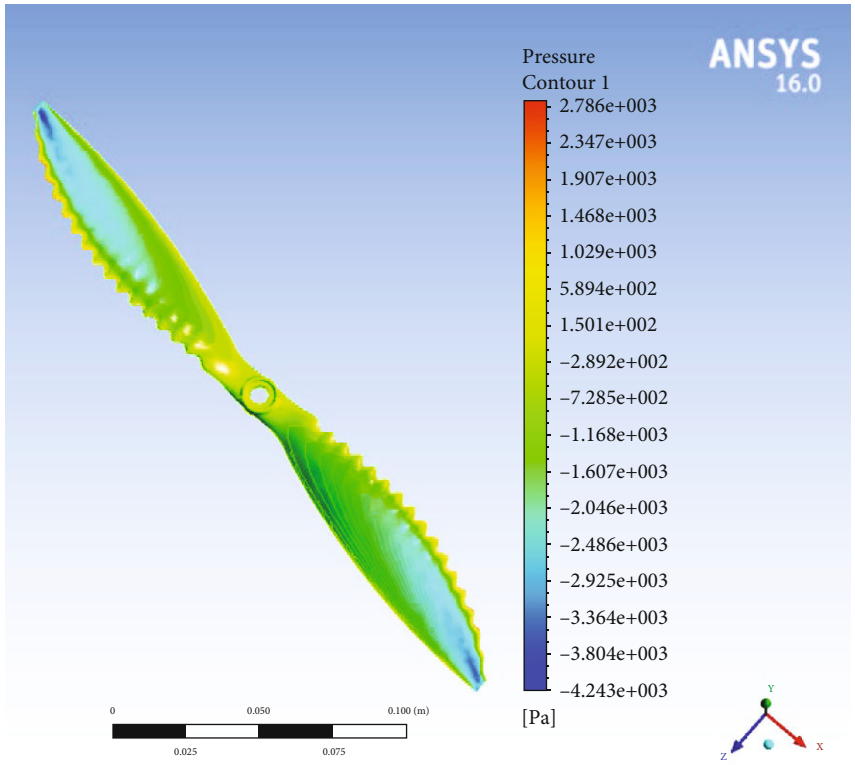

Figure 28: Pressure contour at -100°C temperature.

Table 4: Performance influencing parameters of Design-1.

	Zone-1	Zone-2	Zone-3	Zone-4	Zone-5
Temperature	0°C	-25°C	-50°C	-75°C	-100°C
Diameter (m)	0.254	0.254	0.254	0.254	0.254
Velocity (m/s)	8	8	8	8	8
RPM	5000	5500	6000	6500	7000
J	0.00040640	0.00036946	0.00033867	0.00031262	0.00029029
T	5.6792365	6.4652555	6.8844896	6.9086027	8.8464213
Q	0.0689235	0.0792034	0.10489398	0.10533987	0.13501404
C_t	4.55e-05	4.28e-05	3.83e-05	3.27e-05	3.61e-05
C_p	5.52e-07	2.30e-06	2.30e-06	1.97e-06	2.17e-06
η	0.00532967	2.05e-13	0.000898562	0.000898562	0.000768898

Table 5: Performance influencing parameters of Design-2.

	Zone-1	Zone-2	Zone-3	Zone-4	Zone-5
Temperature	0°C	-25°C	-50°C	-75°C	-100°C
Diameter (m)	0.254	0.254	0.254	0.254	0.254
Velocity (m/s)	8	8	8	8	8
RPM	5000	5500	6000	6500	7000
J	0.00040640	0.00036946	0.00033867	0.00031262	0.00029029
T	604076832	4.4498235	5.00145876	5.984572	7.5842365
Q	0.08756257	0.1058694	0.0586668	0.0135879	0.03658415
C_t	5013e-05	2.95e-05	2.78e-05	2.84e-05	3.10e-05
C_q	7.01e-07	7.67e-10	1.28e-06	2.53e-07	5.86e-07
η	0.04473000	2.57e-01	0.001167508	0.005567677	0.0002433480

Table 6: Performance influencing parameters of Design-3.

	Zone-1	Zone-2	Zone-3	Zone-4	Zone-5
Temperature	0	-25	-50	-75	-100
Diameter (m)	0.254	0.254	0.254	0.254	0.254
Velocity (m/s)	8	8	8	8	8
RPM	5000	5500	6000	6500	7000
J	0.00040640	0.00036946	0.00033867	0.00031262	0.00029029
T	2.4552096	3.2712276	4.2198021	5.1333224	6.0548878
Q	0.7452316	0.0933491	0.11058357	0.09135552	0.15078502
C_t	1.97e-05	2.17e-05	2.35e-05	2.43e-05	2.47-05
C_q	1.57e-10	5.64e-10	5.14e-10	4.54e-10	3.98e-10
η	8.079026632	2.23e+100	2.462487318	2.667694594	2.872901871

7. Conclusion

The aim of the paper is to perform a computational analysis by Ansys 16.0 of newly designed rotor blades at very low temperate conditions (which can fit the atmospheric conditions of Siachen Glacier, in India) which has been achieved. From the obtained pressure contours of Design-1 (Figures 19–23; see Section 6.1) and Design-3 (Figures 24–28, see Section 6.2), it can be clearly found that Design-3 is the best solution for very low-temperature conditions with high-quality pressure distribution around the propeller surface in high altitudes at low-temperature conditions. From the obtained

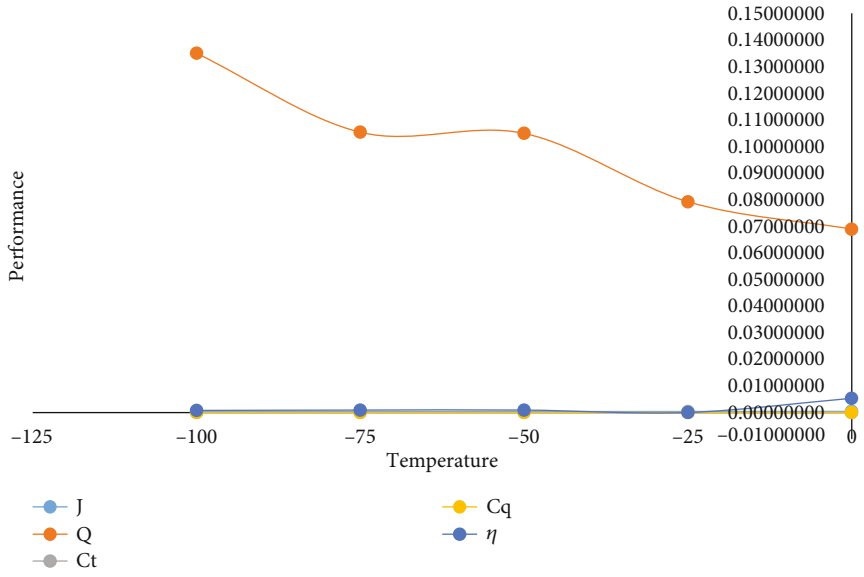

Figure 29: Performance influencing parameters of Design-1.

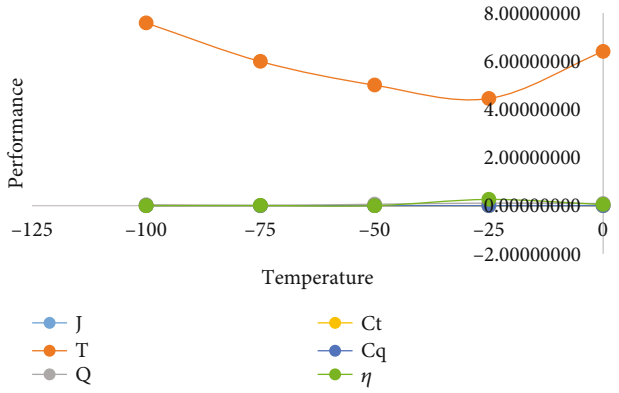

Figure 30: Performance influencing parameters of Design-2.

Table 7: Operational zones vs. propeller efficiency.

	Temperature	Design-1	Design-2	Design-3
Zone-1	0	0.00532963	0.00473462	8.07902663
Zone-2	-25	2.05*e*-13	2.25728004	2.25728004
Zone-3	-50	0.00089856	0.00116751	2.46248732
Zone-4	-75	0.00089856	0.00556768	2.66769459
Zone-5	-100	0.0007689	0.00243348	2.87290187

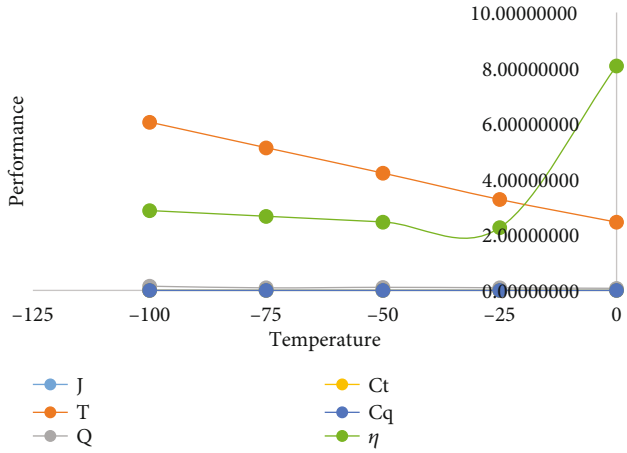

Figure 31: Performance influencing parameters of Design-3.

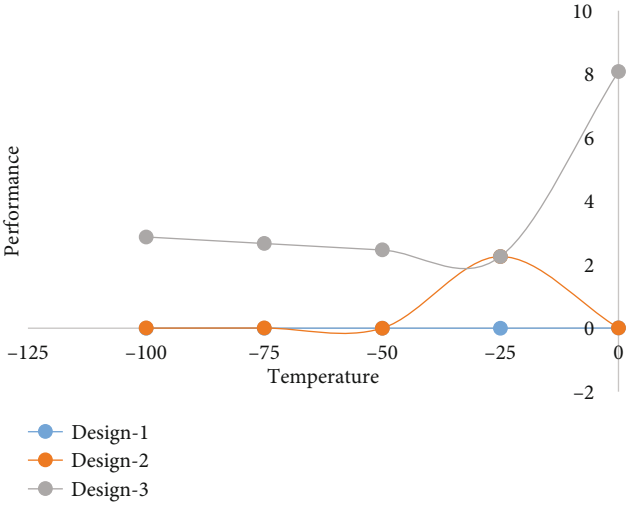

Figure 32: Operational zones vs. propeller efficiency.

values of the performance parameters (J, T, Q, Ct, Cq, and η from Tables 4–6, and Figures 29–31), it can also be found that the values of the thrust coefficient C_t and the efficiency η of Design-3 result in reliable and more durable values

compared to Design-1 and Design-2. Table 7 and Figure 32 show the comparison of the obtained values of the Design-1, Design-2, and Design-3 efficiencies, and as a result of comparison, we can again find that Design-3 is the best design propeller for very low-temperature operational conditions such as in Siachen Glacier, in India. As a continuation of this work, a static structural analysis of Design-3 has been proposed which is going to be presented in the upcoming paper.

Data Availability

(a) Some or all data, models, or code generated or used during the study are available in a repository online in accordance with funder data retention policies. (b) All data, models, and code generated or used during the study appear in the submitted article.

Conflicts of Interest

The authors whose names are listed in this work certify that they have NO affiliations with or involvement in any organization or entity with any financial interest (such as honoraria; educational grants; participation in speakers' bureaus; membership, employment, consultancies, stock ownership, or other equity interest; and expert testimony or patent-licensing arrangements) or nonfinancial interest (such as personal or professional relationships, affiliations, knowledge, or beliefs) in the subject matter or materials discussed in this manuscript.

References

[1] A. Shukla, *846 Indian soldiers have died in Siachen since 1984*, Business-Standard, 2012, Archived from the original on 9 April 2018. Retrieved 13 April 2018 – via Business Standard.

[2] M. E. Brown, H. Ouyang, S. Habib et al., "HIMALA: climate impacts on glaciers, snow, and hydrology in the Himalayan region," *Mountain Research and Development*, vol. 30, no. 4, pp. 401–404, 2010.

[3] https://www.jagranjosh.com/general-knowledge/what-is-the-siachen-glacier-dispute-1528291952-1.

[4] https://www.dailyexcelsior.com/wp-content/uploads/2019/09/page3-23.jpg.

[5] https://keralakaumudi.com/web-news/en/2019/11/NMAN0107123/image/siachen-.1574093958.jpg.

[6] E. Cimoli, M. Marcer, B. Vandecrux, C. E. Bøggild, G. Williams, and S. B. Simonsen, "Application of low-cost UASs and digital photogrammetry for high-resolution snow depth mapping in the Arctic," *Remote Sensing*, vol. 9, no. 11, p. 1144, 2017.

[7] C. De Michele, F. Avanzi, D. Passoni et al., "Microscale variability of snow depth using U.A.S. technology," *The Cryosphere Discussions*, vol. 9, no. 1, pp. 1047–1075, 2015.

[8] Y. Bühler, M. S. Adams, A. Stoffel, and R. Boesch, "Photogrammetric reconstruction of homogenous snow surfaces in alpine terrain applying near-infrared UAS imagery," *International Journal of Remote Sensing*, vol. 38, no. 8-10, pp. 3135–3158, 2017.

[9] M. Korczak-Abshire, A. Zmarz, M. Rodzewicz, M. Kycko, I. Karsznia, and K. J. Chwedorzewska, "Study of Fauna population changes on Penguin Island and turret point oasis (King George Island, Antarctica) using an unmanned aerial vehicle," *Polar Biology*, vol. 42, no. 1, pp. 217–224, 2019.

[10] F. Avanzi, A. Bianchi, A. Cina et al., "Centimetric accuracy in snow depth using unmanned aerial system photogrammetry and a multistation," *Remote Sensing*, vol. 10, no. 5, p. 765, 2018.

[11] C. Jones, J. Ryan, T. Holt, and A. Hubbard, "Structural glaciology of Isunguata Sermia, West Greenland," *Journal of Maps*, vol. 14, no. 2, pp. 517–527, 2018.

[12] J. F. Steiner, F. Pellicciotti, P. Buri, E. S. Miles, W. W. Immerzeel, and T. D. Reid, "Modelling ice-cliff backwasting on a debris-covered glacier in the Nepalese Himalaya," *Journal of Glaciology*, vol. 61, no. 229, pp. 889–907, 2015.

[13] P. Buri, F. Pellicciotti, J. F. Steiner, E. S. Miles, and W. W. Immerzeel, "A grid-based model of backwasting of supraglacial ice cliffs on debris-covered glaciers," *Annals of Glaciology*, vol. 57, no. 71, pp. 199–211, 2016.

[14] F. Brun, P. Wagnon, E. Berthier et al., "Ice cliff contribution to the tongue-wide ablation of Changri Nup Glacier, Nepal, central Himalaya," *The Cryosphere*, vol. 12, no. 11, pp. 3439–3457, 2018.

[15] H. Glauert, *The Elements of Aerofoil and Airscrew Theory*, Cambridge University Press, Cambridge, UK, 1947.

[16] D. O. Dommasch, *Element of Propeller and Helicopter Aerodynamics*, Sir Isaac Pitman & Sons, LTD, 1953.

[17] C. N. Adkins and R. H. Liebeck, "Design of optimum propellers," *Journal of Propulsion and Power*, vol. 10, no. 5, pp. 676–682, 1994.

[18] H. Glauert, *Aerodynamic Theory*, Springer, Berlin, Heidelberg, 1935.

[19] C. Burger, *Propeller Performance Analysis and Multidisciplinary Optimization using a Genetic Algorithm, [Ph.D. thesis]*, Auburn University, 2007.

[20] B. M. Kulfan, "Universal parametric geometry representation method," *Journal of Aircraft*, vol. 45, no. 1, pp. 142–158, 2008.

[21] W. C. Nelson, *Airplane Propeller Principles*, John Wiley and Sons, 1944.

[22] F. E. Weick, *Aircraft Propeller Design*, McGraw-Hill, 1930.

[23] http://www.aerodynamics4students.com/propulsion/blade-element-rotor-theory.php.

[24] https://www.aircraftsystemstech.com/2017/04/aircraft-propellers.html.